Journal of Materials Chemistry A

Accepted Manuscript

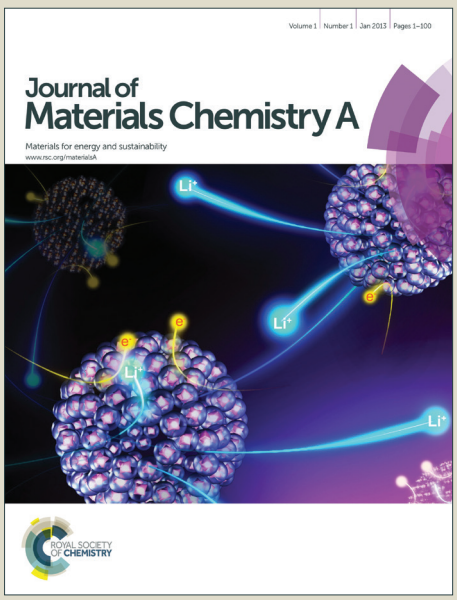

ROYAL SOCIETY OF CHEMISTRY

www.rsc.org/materialsA

Journal Name
Journal of Materials Chemistry A
Dynamic Article Links ►

Cite this: DOI: 10.1039/c0xx00000x

www.rsc.org/xxxxxx

ARTICLE TYPE

Three-Dimensional Graphitic Carbon Nitride Functionalized Graphene-Based High-Performance Supercapacitors

Qing Chen, Yang Zhao, Xianke Huang, Nan Chen,* and Liangti Qu*

Received (in XXX, XXX) Xth XXXXXXXXX 20XX, Accepted Xth XXXXXXXXX 20XX
DOI: 10.1039/b000000x

Three-dimensional graphitic carbon nitride functionalized graphene composites (g-C_3N_4@G) were grown using a simply one-step hydrothermal reduction. The super-capacitive properties of the as-formed 3D g-C_3N_4@G were evaluated in a symmetrical supercapacitor. It is found that the 3D g-C_3N_4@G exhibit high specific capacitance of 264 $F\cdot g^{-1}$ and good cycling stability.

Introduction

Electrochemical supercapacitors (ECs) have attracted increasing attentions, especially in the fields of electrochemical energy storage and conversion due to their high power capability and long cycle-life.[1-3] ECs can be divided into two types, electric double layer capacitors (EDLCs) and the pseudo-capacitors. The electrodes for EDLCs capacitor are usually the materials with high surface area through the separation of electronic and ionic charges at the electrode-electrolyte interface. While the pseudo-capacitors are based on redox active electrode materials (e.g., metal oxides, conducting polymers, and carbons rich in oxygen and nitrogen containing surface functional groups) that operate through fast and reversible surface or near-surface Faradic reactions.[4-6] To achieve a high performance of ECs, the electrode materials are allowed to possess large specific surface area, high conductivities, low fabrication cost, abundant resource and satisfactory electrochemical stability. Among the various kinds of electrode materials applied into ECs, carbon-based materials with high effective surface area and excellent conductivity have received much attentions recently.[7,8] To meet the increasing demands for reliable efficient energy storage devices, the development of new promising materials with high energy storage still remains challenging.

Graphitic carbon nitride (g-C_3N_4), a two-dimensional (2D) graphite-like structure, has attracted considerable attention owing to its high nitrogen content, excellent chemical and thermal stability, special optical features, appealing electronic structure and environmental friendly feature, thus leading to multifunctional catalytic activities for photocatalysis and other energy conversion process.[9-13] g-C_3N_4 is mainly restricted in the electrochemical-related applications due to the inherent low electronic conductivity and low surface area.

Graphene with a 2D monolayer structure of sp^2-bonded carbon atoms has many advantages over other carbon materials such as large specific surface area, outstanding electrical, mechanical and thermal properties.[14,15] As is well known graphene can be used as a versatile building block for self-assembling into specific architectures, which is essential for converting the remarkable microscopic characteristics of graphene sheet into macroscopic properties of practical significance.[16,17] It was found that the combination of g-C_3N_4 with graphene could improve the conductivity and electrocatalytic performance of g-C_3N_4, which has been explored as a metal-free material for electrocatalysis.[18] In this work, we have reported a rational assembly of g-C_3N_4 and graphene into 3D interconnected networks y a facile one-step hydrothermal method. The resulting well-defined 3D g-C_3N_4@G induces the hierarchical architecture, thus facilitate the charge transfer and provide multi-way electron transfer which can effectively accelerate the electrochemical process to achieve high energy storage.

Consequently, the as prepared g-C_3N_4@G exhibits a significantly enhanced electrochemical capacitance of 264 $F\cdot g^{-1}$ at 0.4 $A\cdot g^{-1}$, representing a nearly more than 75 % capacitance improved in comparison to the pristine graphene hydrogels (152 $F\cdot g^{-1}$).

Experimental

Preparation of Graphene Oxide

Graphene Oxide (GO) was prepared by oxidation of natural graphite powder according to a modified Hummers' method. Briefly, graphite (3g) was added to concentrated sulfuric acid (70 mL) under stirring at room temperature, then sodium nitrate (1.5 g) was added, and the mixture was cooled to 0 °C. Potassium permanganate was added slowly to keep the temperature of the suspension lower than 20 °C under vigorous agitation. The reaction system was transferred to a 35-40 °C water bath for about 0.5 h, forming a thick paste. 140 mL water was added and keep agitation for 15min, then an additional 500 mL of water was added and followed by a slow addition of 20 mL of H_2O_2 (30 %), turning the color of the solution from dark brown to yellow. The mixture was filtered and washed with 1:10 HCl aqueous solution (250 mL) to remove metal ions followed by repeated washing with water and centrifugation to remove the acid. The resulting solid was dispersed in water by ultrasonication for 1 h to make a GO aqueous dispersion (0.5 wt. %). Finally, the obtained brown

dispersion was subjected to 30 min of centrifugation at 4000 rpm to remove any aggregates.[19]

Preparation of g-C_3N_4

This preparation used melamine as the precursor, which was carbonized at 600 °C for 2 h in a quartz tube furnace and treated with concentrated sulfuric acid. And then, the as-produced g-C_3N_4 were exfoliation with an excess of $KMnO_4$ at 50 °C for 2h, H_2O_2 (30 %) was added to remove the surplus of $KMnO_4$ from the sphere of the reaction. Finally, the product was purified by dialysis and freeze-drying for further use.

Preparation of 3D g-C_3N_4@G

3D g-C_3N_4@G was prepared by hydrothermal reduction of GO sheets and g-C_3N_4 in their mixed aqueous dispersion. According to experimentation and data comparison as shown in the supporting information, 2 mg g-C_3N_4 was dispersed into 15 mL homogeneous GO aqueous (3 mg·mL^{-1}) under stirring in a beaker. Then the mixture was transferred to the Teflon-lined autoclave at 180 °C for 12 h, the 3D-structure was finally obtained through lyophilization for following experiments.

Fabrication of g-C_3N_4@G supercapacitors

All the components were directly assembled into a layered structure without using a binding agent or conducting additive. The two slices of g-C_3N_4@G electrodes (*ca.* 0.5 mm × 2 mm × 2 mm), that cut from the as-prepared cylindrical g-C_3N_4@G sample, were separated by a piece of filter paper soaked with 0.1 M $LiClO_4$ electrolyte and thus assembled in a symmetrical two-electrode configuration with gold flakes of 0.3 × 0.5 cm as the current collector to fabricate a symmetrical supercapacitor.

Electrochemical Measurements

Electrochemical performances of the supercapacitor were tested with galvanostatic charge-discharge and cyclic voltammetry (CV) on a CHI 760 potentiostat, CH Instruments, Inc. All of the experiments were carried out in a two-electrode system. The potential range for CV measurements and galvanostatic charge/discharge tests have been performed in a potential range between 0 and 1 V, the electrochemical impedance spectra (EIS) were taken at the open-circuit potential in the frequency range of 0.01-10^5 Hz with a modulating amplitude of 5 mV. The capacitance C was calculated by using the equation: C = I/(dV/dt), where I and dV/dt are the discharge current and the slope of the discharge curve. The mass-specific capacitances (C_m) was derived from the equation: $C_m = 2C/m$, m is the mass of one electrode. The energy density (E) and Power density (P) of the g-C_3N_4@G supercapacitor depicted in the Ragone plot was calculated by the equation $E=0.5C_m\triangle V^2$ and $P=E/\triangle t$, where $\triangle t$ was the discharge time, $\triangle V$ was the voltage change within the discharge time.[20]

Characterization

The morphology of the samples was explored by JSM-7001F Field-emission scanning electron microscope (FE-SEM) and JEM-2010 high resolution transmission electron microscopy (HR-TEM). The X-ray diffraction (XRD) analysis was carried on D8 advance X-ray diffractometer with Cu Ka radiation (λ=1.5418 Å). FT-IR spectrum is recorded from KBr pellets in range 400-4000 cm^{-1} on a Nicolet-360 FT-IR spectrometer. X-ray photoelectron spectroscopy (XPS) analysis was performed on the ESCALAB 250 photoelectron spectrometer (ThermoFisher Scientific) with Al Ka (1486.6 eV) as the X-ray source set at 150 W and a pass energy of 30 eV for high-resolution scan. Conductivities of the samples were measured by a conventional four-probe technique. Nitrogen sorption measurements were carried out with a Quantachrome Autosorb-IQ gas adsorption analyzer at 77 K.

Results and Discussion

The process for the fabrication of 3D g-C_3N_4@G is illustrated in **Figure 1a**. The hydrothermal treatment process allows formation of g-C_3N_4 grafted graphene basal plane with a loosely 3D structure with a density of 13.2 mg cm^{-3} as shown in **Figure 1b** and **1c** similar to that of common 3D graphene (Figure S1).[17] The enlarged SEM image in **Figure 1d** reveals that g-C_3N_4 in the composites are uniformly dispersed along graphene basal planes without any obvious aggregates which is further confirmed by the corresponding EDS elemental mapping (**Figure 1e**). Elemental mappings clearly show that the uniform distribution of N, C, and O elements over the graphene mesh. The conductivity of g-C_3N_4@G (0.38 S·m^{-1}) is comparable to the pristine graphene (0.35 S·m^{-1}). Meanwhile, the nitrogen cryo-adsorption isotherms are shown in (Figure S2), where both 3DG and g-C_3N_4@G composites show a Type IV isotherm characteristics with a wide hysteresis loop indicating the existence of mesopores. Pore size distribution curves reveal a narrow distribution of pores diameters, the specific surface area of g-C_3N_4@G deposition is 320 m^2·g^{-1}, which is obviously higher than that of the pristine 3D graphene (208 m^2·g^{-1}).

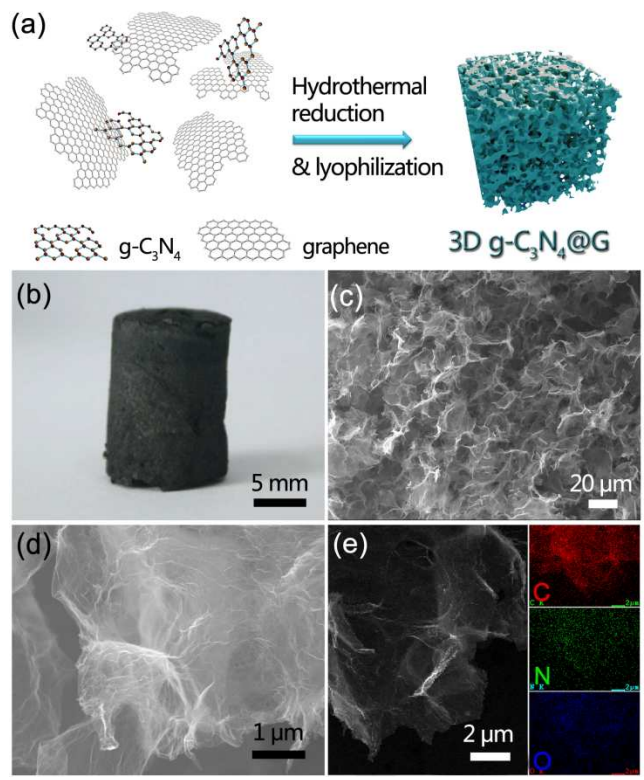

Figure 1. (a) Progress on preparation of 3D g-C_3N_4@G; (b)

photograph of g-C_3N_4@G; (c) SEM image of g-C_3N_4@G and (d) the corresponding enlarged SEM image of (c); (e) the samples were characterized by EDS elemental mapping.

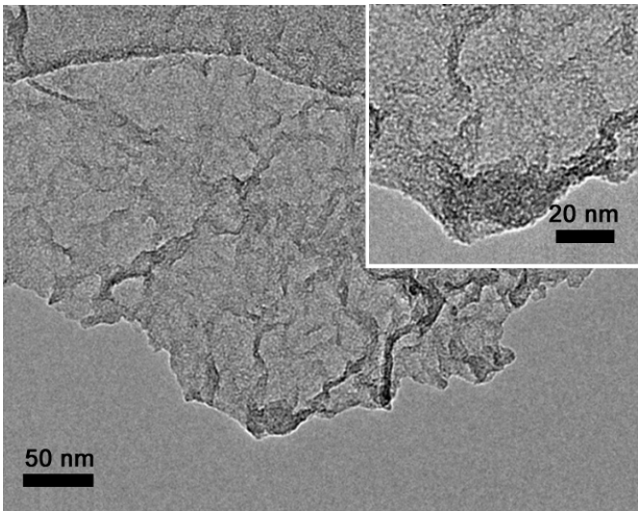

Figure 2. TEM image and of g-C_3N_4@G, the inset is the HRTEM of g-C_3N_4@G.

XPS measurement further verifies the existence of C 1s peak, along with an N 1s peak corresponding to an N content of 11.44 at. % and a weak O 1s peak without any impurities (**Figure 3a**). As shown in **Figure 3b**, the high-resolution C 1s spectrum exhibits the chemical relationships of the carbon. The peak at 284.8 eV belongs to C-C coordination, and the peak centered at 288.3 eV corresponds to C-N coordination of g-C_3N_4. The high-resolution N 1s spectrum (**Figure 3c**) reveals the typical nitrogen status including pyridine (398.8 eV), pyrrolic (400.5 eV), and graphitic (401.1 eV) N species, which are also reflected by C-N-C peak in the C 1s spectrum of g-C_3N_4@G (**Figure 3b**).

Figure 3d shows the XRD patterns of g-C_3N_4@G in comparison with original g-C_3N_4 and pristine graphene. A broad peak at ca. 25° that observed in graphene is a characteristics belonging to the (002) peak of graphitic carbon planes, indicating a similar interlayer spacing of 0.34 nm in graphene obtained from XRD pattern with other common fabricated graphene materials. The original g-C_3N_4 represents a sharp diffraction peak at about 27.3° corresponding to the (002) peak of g-C_3N_4 due to interlayer stacking reflection of conjugated aromatic systems,[21, 22] the peak of g-C_3N_4@G shifted to 26.4°, suggesting that a composite structure can be obtained by the intermolecular π–π stacking interaction between graphene layer and g-C_3N_4 depend on well-distribution with the hydrothermal treatment. The result is in agreement with the STEM observations as shown in **Figure 2**.

The g-C_3N_4@G were also characterized by FT-IR spectrum as shown in **Figure 3e**. The original g-C_3N_4 exhibit typical C-N heterocyclic stretches of triazine ring in the *ca.* 1100-1700 cm^{-1} region. The sharp absorption at *ca.* 800 cm^{-1} belongs to deformation of tri-s-triazine ring modes. The peaks at *ca.* 3200 and 3400 cm^{-1} can be attribute to stretching and deformation modes of -NH_2 groups. While, the typical peaks of graphene at ~1200 cm^{-1}, ~1623 cm^{-1}, and 3040 cm^{-1} can be assigned to the C-OH, C=C, and O-H stretching vibration modes, respectively.[23] Although most of the characteristic peaks of CN heterocycles of g-C_3N_4 in the g-C_3N_4@G are overlapped by graphene, the peaks at *ca.* 800 cm^{-1} and *ca.* 1571 cm^{-1} belonging to g-C_3N_4 can still be recognized.[24, 25]

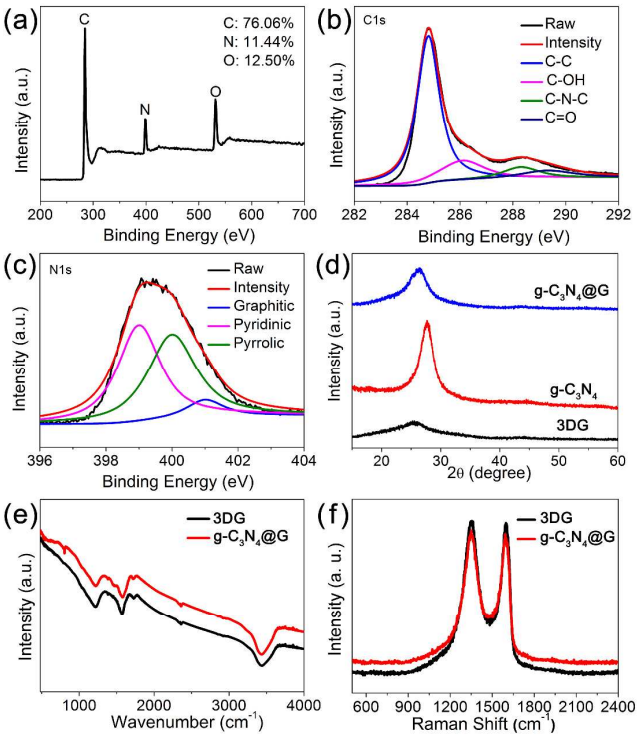

Figure 3. (a) XPS survey spectrum of g-C_3N_4@G; (b) The corresponding high-resolution C 1s spectrum and (c) N 1s spectrum; (d) XRD patterns of the original g-C_3N_4, pristine graphene, and g-C_3N_4@G; (e) FT-IR spectrum of the 3DG and g-C_3N_4@G, respectively; (f) Raman spectrum of the 3DG and g-C_3N_4@G.

The electrochemical performance of g-C_3N_4@G were measured in a two-electrode configuration. To ascertain the origin of the exceptional performance of the g-C3N4@G-based supercapacitor, we also tested the electrochemical performance of the pristine graphene for comparison. A symmetric supercapacitor was approximated constructed by first sandwiching the membrane that soaked with 0.1 $mol \cdot L^{-1}$ of $LiClO_4$ between two identical pieces of g-C_3N_4@G, and then encapsulating the device with porous polyethylene terephthalate (PET) membranes (**Figure 3a**). The CV curves of g-C_3N_4@G capacitor with the potential range from 0 to 1.0 V (vs. Ag/AgCl) exhibit almost rectangular-like shape indicating a good charge transport within the g-C_3N_4@G electrodes as shown in **Figure 4b**, the scan rate is 10, 30, 50, and 100 $mV \cdot s^{-1}$, respectively. The galvanostatic charge/discharge curves with different current densities of 0.4, 1.0, 2.0, 3.0, and 4.0 $A \cdot g^{-1}$ were shown in **Figure 4c**, no obvious IR drop was observed on the start of all discharge curves, indicating that all the devices had a small internal series resistance and efficient extraction of stored energy. The specific capacitance of the g-C_3N_4@G was calculated to be about 264 $F \cdot g^{-1}$ at a current density of 0.4 $A \cdot g^{-1}$ based on the charge–discharge curves, which is the best value the survey of supercapacitors based on 3DG has recorded (**Table 1**). Notably, the capacitance

of g-C_3N_4@G electrode was about twice as high as the 3D pristine graphene electrode at a range of current densities from 1.0 to 4.0 A·g^{-1} (**Figure 4e**). This essentially implies g-C_3N_4@G have a larger active surface areas and faster electron transfer rate in comparison with the control electrode.

Electrochemical impedance spectroscopy (EIS) was also performed to further evaluate the electrochemical performance of devices based on 3DG and g-C_3N_4@G, respectively. Both devices show characteristics approaching the ideal capacitive behavior (**Figure 4f**). The high-frequency intercept with the real axis is the equivalent series resistance (Rs), representing the sum of the electrolyte solution resistance, the intrinsic resistance of active material and the contact resistance at the electrode/electrolyte interface.[26] It is clearly observed that the g-C_3N_4@G has a slightly lower Rs value than that of 3DG from the magnified high-frequency region in the inset image. The power density and energy density are caculated by using the charge-discharge data. **Figure 4g** shows the Ragone plot for g-C_3N_4@G based supercapacitor. The energy density is nearly 30 W·h·kg^{-1} and the power density is 4.0 kW·kg^{-1} at a current density of 4.0 A·g^{-1}, these results indicate that the supercapacitor based on g-C_3N_4@G material can operate with higher power density and energy density.[7, 27]

Table 1. Direct comparison of the specific capacitance (C_m) of different 3DG-based materials supercapacitors

No.	Category	Electrode materials	C_m (F g^{-1})	Ref.
1		g-C_3N_4@G	264	this work
2		silver nanoparticles decorated graphene foam	110	28
3		graphene-polyoxometalate nanomaterials	123	29
4	Graphene-metal oxide	In_2O_3/reduced GO	178	30
5		MnO_2 deposited on GO	216	31
6		$Ni(OH)_2$/graphene and porous graphene	218.4	32
7		3D MnO_2/graphene hydrogel	242	33
8	Graphene-organic/polymer	pyrene carboxylic acid functionalized graphene foam	133	34
9		surfactant-modified GO	168	35
10		graphene/polypyrrole nanotube hybrid aerogel	253	36
11		3D N-doped graphene-CNT networks	180	37
12		C_{60}/graphene composite	135	38

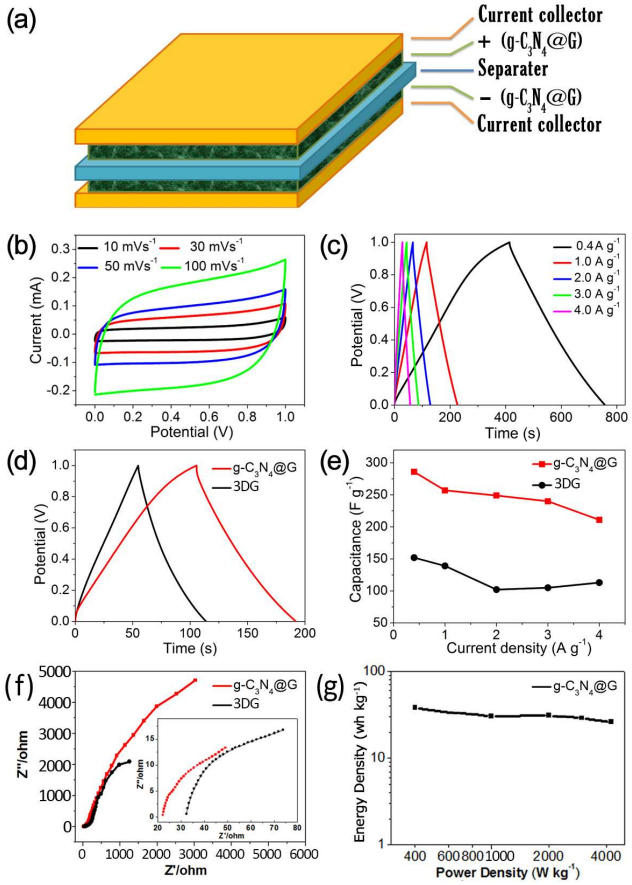

Figure 4. (a) Schematic illustration of g-C_3N_4@G supercapacitor device; (b) CV curves with different scan rates and (c) galvanostatic charge-discharge curves for g-C_3N_4@G at different discharge current densities; (d) The galvanostatic charge-discharge curves of graphene and g-C_3N_4@G with the currents density of 1.0 A·g^{-1}; (e) Capacitance at different current densities of g-C_3N_4@G and graphene; (f) Nyquist plots of g-C_3N_4@G and graphene measured at open-circuit conditions, high-frequency region of the plots are shown enlarged in the inset image; (g) Ragone plot of g-C_3N_4@G based supercapacitor.

Figure 5a and **5b** described the CV and charge/discharge curves of g-C_3N_4@G supercapacitor after 1,000 charge-discharge cycles test with the current density of 3.0 A·g^{-1}. The CV carves show similar rectangular shapes, current densities at all scan rates, and galvanostatic charge-discharge time as its initial-status, indicating a nearly ideal supercapacitor behavior of the supercapacitor and a desirable fast charge-discharge property. This data assuredly suggests that the g-C_3N_4@G supercapacitor offers larger discharge capacity after 1000 charge-discharge cycles than before, which is consistent with the CV results.

The charge/discharge specific capacitance values of the g-C_3N_4@G supercapacitor at the different current densities after 1,000 charge-discharge cycles exhibits a specific capacitance as high as 286 F·g^{-1} at a discharge current density of 0.4 A·g^{-1} (as shown in **Figure 5c**). Moreover, the capacitance of this sample still remained at 211 F·g^{-1} at a high current density of 4.0 A·g^{-1}. As we all know, the diffusion of ion from the electrolyte can gain access to the maximum surface area of the active materials at the lower current density, therefore a higher specific capacitance can be attained. With the increment of current density, the effective

interaction between the ions and electrode is reduced resulting in a reduction in capacitance. It can be seen that the specific capacitance values after 1000 charge-discharge cycles was obvious higher than its initial status at all the current densities, this may be caused by the fact that the g-C_3N_4@G was activated for being long time charge-discharge.

The cycling stability of the supercapacitor is also an important parameter to evaluate its potential for practical applications. **Figure 5d** illustrates the temporal evolution of the specific capacitance of g-C_3N_4@G supercapacitor over consecutive charge-discharge cycles. Interestingly, the specific capacitances increases at the first several hundred cycles, then gradually decrease and eventually stabilize. The increase of during initial cycles can be attributed to the activation process that allows the trapped ions to diffuse out. There is no obvious degradation could be observed during the cycling experiment even after 10000 charge-discharge cycles, indicating that our g-C_3N_4@G supercapacitor has a good long-term electrochemical stability.

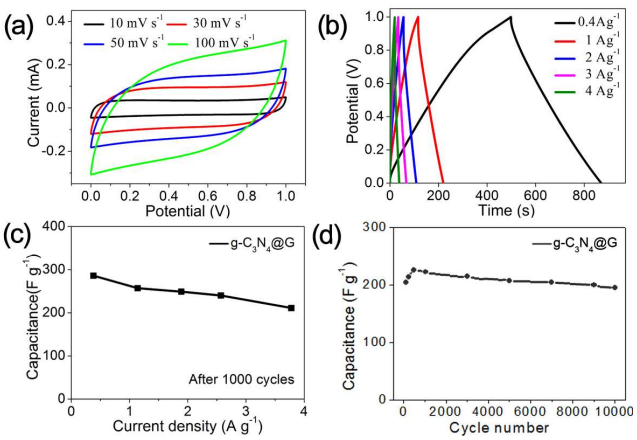

Figure 5. (a) CV curves of supercapacitors based on the g-C_3N_4@G after 1000 charge-discharge cycles with the current density at 3.0 $A\cdot g^{-1}$, scan rates are 10 $mV\cdot s^{-1}$, 30 $mV\cdot s^{-1}$, 50 $mV\cdot s^{-1}$ and 100 $mV\cdot s^{-1}$, respectively; (b) The galvanostatic charge-discharge curves of g-C_3N_4@G supercapacitor after 1000 charge-discharge cycles at different discharge currents: 0.4, 1.0, 2.0, 3.0, and 4.0 $A\cdot g^{-1}$; (c) The capacitance of g-C_3N_4@G supercapacitor after 1000 charge-discharge cycles; (d) The capacitance of g-C_3N_4@G supercapacitor under the cycling tests for 10000 charge-discharge cycles at a current density 4.0 A g^{-1}.

Conclusions

In summary, g-C_3N_4@G have been prepared by a simply one-step hydrothermal reduction and showed promising electrochemical performances as electrode materials for supercapacitor. The results showed that the existence of g-C_3N_4 was advantageous in that it could decrease the aggregation of graphene, leading to a capacity improvement and better cycle performance. Capacitance values of 264 $F\cdot g^{-1}$ have been achieved representing a more than 75% improvement over that of the supercapacitor made from pure 3DG electrodes (152 $F\cdot g^{-1}$). The reported 3D composites materials are much desirable for electrode materials in supercapacitors.

Acknowledgements

This work is sponsored by NSFC (No. 21325415, 21174019, 21301018), National Basic Research Program of China (2011CB013000), Beijing Natural Science Foundation (2152028), Fok Ying Tong Education Foundation (No. 131043) and the 111 Project B07012.

Notes and references

[a] *Key Laboratory of Cluster Science, Ministry of Education of China; Beijing Key Laboratory of Photoelectronic/Electrophotonic Conversion Materials;*
School of Chemistry, Beijing Institute of Technology, Beijing 100081, China; E-mail: gabechain@bit.edu.cn; lqu@bit.edu.cn

† Electronic Supplementary Information (ESI) available: [details of any supplementary information available should be included here]. See DOI: 10.1039/b000000x/

‡ Footnotes should appear here. These might include comments relevant to but not central to the matter under discussion, limited experimental and spectral data, and crystallographic data.

1 Z. L. Wang, and J. H. Song, *Science*, 2006, **312**, 242.
2 Z. S. Wu, D. W. Wang, W. C. Ren, J. P. Zhao, G. M. Zhou, F. Li and H. M. Cheng, *Adv. Funct. Mater.*, 2010, **20**, 3595.
3 Q. Chen, Y. Hu, C. G. Hu, H. H. Cheng, Z. P. Zhang, H. B. Shao and L. T. Qu, *Phys. Chem. Chem. Phys.*, 2014, **16**, 19307.
4 P. Simon and Y. Gogotsi, *Nat. Mater.*, 2008, **7**, 845.
5 N. Lin, J. H. Tian, Z. Q. Shan, K. Chen and W. M. Liao, *Electrochim. Acta*, 2013, **99**, 219.
6 H. M. Jeong, J. W. Lee, W. H. Shin, Y. J. Choi, H. J. Shin, J. K. Kang and J. W. Choi, *Nano Lett.*, 2011, **11**, 2472.
7 Y. M. Tan, C. F. Xu, G. X. Chen, Z. H. Liu, M. Ma, Q. J. Xie, N. F. Zheng and S. Z. Yao, *ACS Appl. Mater. Interfaces*, 2013, **5**, 2241.
8 T. Y. Kim, G. J. Jung, S. Yoo, K. S. Suh and R. S. Ruoff, *ACS Nano*, 2013,**7**,6899.
9 Y. Zheng, J. Liu, J. Liang, M. Jaroniec and S. Z. Qiao, *Energy Environ. Sci.*, 2012, **5**, 6717.
10 M. Groenewolt and M. Antonietti, *Adv. Mater.*, 2005, **17**, 1789.
11 X. C. Wang, K. Maeda, X. F. Chen, K. Takanabe, K. Domen, Y. D. Hou, X. Z. Fu and M. Antonietti, *J. Am. Chem. Soc.*, 2009, **131**, 1680.
12 Y. Hou, Z. H. Wen, S. M. Cui, X. Guo and J. H. Chen, *Adv. Mater.*, 2013, **25**, 6291.
13 S. Yang, Y. Gong, J. Zhang, L. Zhan, L. Ma, Z. Fang, R. Vajtai, X. C. Wang and P. M. Ajayan, *Adv. Mater.*, 2013, **25**, 2452.
14 K. Geim and K. S. Novoselov, *Nat. Mater.*, 2007, **6**, 183.

15 K. S. Novoselov, A. K. Geim, S. V. Morozov, D. Jiang, Y. Zhang, S. V. Dubonos, I. V. Grigorieva and A. A. Firsov, *Science*, 2004, **306**, 666.

16 Y. Zhao, C. G. Hu, L. Song, L. X. Wang, G. Q. Shi, L. M. Dai and L. T. Qu, *Energy Environ. Sci.*, 2014, **7**, 1913.

17 Y. Zhao, C. G. Hu, Y. Hu, H. H. Cheng, G. Q. Shi and L. T. Qu, *Angew. Chem. Int. Ed.*, 2012, **51**, 11371.

18 J. Liang, Y. Zheng, J. Chen, J. Liu, H. J. Denisa, M. Jaroniec and S. Z. Qiao, *Angew. Chem. Int. Ed.*, 2012, **51**, 3892.

19 Y. X. Xu, K. X. Sheng, C. Li and G. Q. Shi, *ACS Nano*, 2010, **4**, 4324.

20 Y. N. Meng, Y. Zhao, C. G. Hu, H. H. Cheng, Y. Hu, Z. P. Zhang, G. Q. Shi and L .T. Qu, *Adv. Mater.*, 2013, **25**, 2326.

21 D. Q. Gao, Q. Xu, J. Zhang, Z. L. Yang, M. S. Si, Z. J. Yan and D. S. Xue, *Nanoscale*, 2014, **6**, 2577.

22 F. Dong, L. Wu, Y. Sun, M. Fu, Z. Wu and S. C. Lee, *J. Mater. Chem.*, 2011, **21**, 15171.

23 X. J. Lua, H. Dou, C. Z. Yuan, S. D. Yang, L. Hao, F. Zhang, L. F. Shen, L. J. Zhang and X. G. Zhang, *J. Power Sources*, 2012, **197**, 319.

24 Y. Zhao, Z. Liu, W. Chu, L. Song, Z. Zhang, D. Yu, Y. Tian, S. Xie, and L. Sun, *Adv. Mater.*, 2008, **20**, 1777.

25 L. Xu, J. X. Xia, H. Xu, S. Yin, K. Wang, L. Y. Huang, L. G. Wang and H. M. Li, *J. Power Sources*, 2014, **245**, 866.

26 H. M. Sun, L. Y. Cao and L. H. Lu, *Energy Environ. Sci.*, 2012, **5**, 6206.

27 T. Christen and M. W. Carlen, *J. Power Sources*, 2000, **91**, 210.

28 A. Bello, M. Fabiane, D. Dodoo-Arhin, K. I. Ozoemena and N. Manyala, *J. Phys. Chem. Sol.*, 2014, **1**, 109.

29 S. G. Jullieth, R. Vanesa and G. R. Pedro, *Phys. Chem. Chem. Phys.*, 2014, **16**, 20411.

30 X. Y. Xu, T. Wu, F. L. Xia, Y. Li, C. C. Zhang, L. Zhang, M. X. Chen, X. C. Li, L. Zhang and Y. Liu, *J. Power Sources*, 2014, **266**, 282.

31 C. Z. Yuan, L. Yang, L. R. Hou, L. F. Shen, X. G. Zhang and X. W. Lou, *Energy Environ. Sci.*, 2012, **5**, 7883.

32 G. H. Yu, L. B. Hu, N. A. Liu, H. L. Wang, M. Vosgueritchian, Y. Yang, Y. Cui and Z. A. Bao, *Nano Lett.*, 2011, **11**, 4438.

33 S. S. Wu, W. F. Chen and L. F. Yan, *J. Mater. Chem. A*, 2014, **2**, 2765.

34 A. Bello, M. Fabiane, D. Y. Momodu, S. Khamlich, J. K. Dangbegnon, N. Manyala, *J. Solid State Electrochem.*, 2014, **18**, 2359.

35 Q. Q. Ke, Y. Q. Liu, H. J. Liu, Y. Zhang, Y. T. Hu and J. Wang, *RSC Adv.*, 2014, **4**, 26398.

36 S. B. Ye and J. C. Feng, *ACS Appl. Mater. Interf.*, 2014, **6**, 9671.

37 B. You, L. L. Wang, L. Yao and J. Yang, *Chem. Commun.*, 2013, **49**, 5016.

38 J. Ma, Q. Guo, H. L. Gao and X. Qin, *Fuller. Nanotub. Car. N.*, 2015, **23**, 477.

One-step strategy to graphitic-C3N4 functionalized graphene composites as advanced three-dimensional supercapacitor electrode materials.

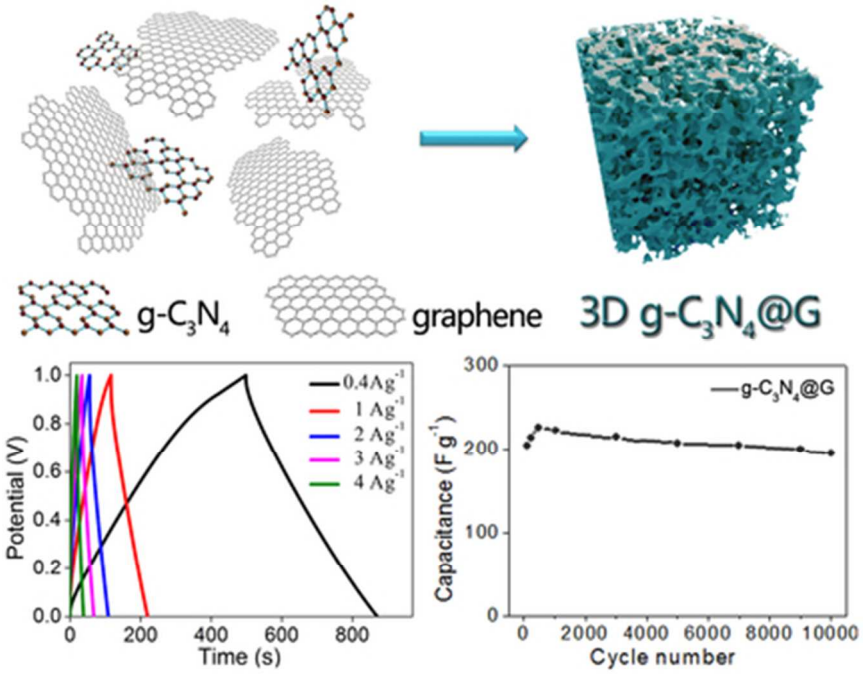

36x28mm (300 x 300 DPI)